Modified single fiber fragmentation test procedure to study water degradation of the fiber/matrix interface toughness of glass/vinylester

Felipe A. Ramirez · Leif A. Carlsson

Abstract A modified single fiber fragmentation test (SFFT) procedure, that permits separation of the fiber break and fiber/matrix (F/M) debond propagation events, was employed to characterize the (F/M) interface toughness of dry and water saturated E-glass/vinylester. By focusing solely on the debond propagation event, and by measuring the critical load for debond propagation, fracture mechanic analysis enabled determination of the fracture toughness of the fiber/matrix interface. After immersion in seawater, the interface was substantially degraded. The fracture toughness was reduced by approximately a factor of two.

Introduction

Fiber reinforced polymer matrix composites are used in several structural applications since they offer several advantages over traditional materials such as metals, ceramics, and plastics. Moisture absorption, however, is a common scenario which may lead to a number of undesirable effects, such as degradation of fiber, matrix, and fiber/matrix (F/M) interface.

In the study of polymer composite durability, more focus is on the fiber/matrix interface region since the structural integrity and lifetime of polymer composites are critically dependent on the stability of the F/M interface [1, 2]. Therefore, it is extremely important to characterize the F/M interface to understand the overall performance of polymer matrix composites. The single fiber fragmentation test (SFFT) is one of the most popular tests used to evaluate the fiber/matrix adhesion. The SFFT consists of a single fiber embedded in a resin matrix molded into a dog-bone shaped specimen. As the SFFT specimen is loaded in tension, the fiber will be loaded through an interfacial shear stress transfer mechanism (shear-lag) [3], and break into several fragments until no further breaks occur. This state is called fiber break saturation, and the final fiber fragmentation length is referred to as the *critical length*, $2L_c$ [4] (L_c at each side of the fiber break). A stronger bond between fiber and matrix enables more transfer of load into the fiber which results in a shorter critical fragment length.

Several models such as the Kelly–Tyson shear lag analysis [4] use the critical length to determine the F/M interface shear strength [4, 5]. The Kelly–Tyson model, however, assumes a constant shear stress along the F/M interface and does not account for other failure processes that are observed such as F/M interface shear failure (debonding) [6–8]. Therefore, several other models [9–14] have been proposed and utilized to characterize the F/M interface by the use of an interface fracture toughness quantity such as the energy release rate for propagation of an interface debond. These fracture models, however, combine the debond propagation event and the fiber break event, and separation of the individual energy contributions is not straight-forward since analysis of the fiber failure event must consider the dynamic unloading of the fiber ligaments after the fiber breaks.

In order to accurately determine the fiber/matrix interface fracture toughness, a revised SFFT procedure and associated fracture mechanics analysis that isolates the event of debond growth were recently proposed by Ramirez et al. [15]. The revised SFFT procedure consists of loading the specimen under a microscope until the first fiber break and associated instantaneous F/M debonding occur. Following these events, the specimen is unloaded and then

F. A. Ramirez (✉) · L. A. Carlsson
Department of Mechanical Engineering, Florida Atlantic University, 777 Glades Road, Boca Raton, FL 33431, USA
e-mail: feliperamirez17@gmail.com

loaded again until the existing debond is observed to grow. Based on the critical load, the energy release rate for debond propagation is determined.

The aim of this work is to utilize a revised single fiber fragmentation test to quantify the degradation of the F/M interface toughness by water absorption, and compare the results to interface shear strengths determined at dry and wet conditions using the traditional SFFT.

Experimental

Materials and specimens

The SFFT employs a single fiber embedded in a resin matrix which is molded into a dog-bone specimen as shown in Fig. 1 [16]. A rubber modified vinylester system, Ashland Derakane vinylester 8084 (VE D8084), was used as the matrix. The matrix was cured for 24 h at room temperature followed by a 2 h post cure at 99 °C. The fiber was an E-glass fiber obtained from 3TEX with silane sizing. The properties of fiber and matrix [7, 17, 18] are listed in Table 1. Note that previous experiments [7] showed that the modulus and glass transition temperature of the vinylester matrix used here are not significantly impacted by water exposure.

Environmental exposure

After post-cure of the specimens, they were considered dry (defining dry conditions). A number of the specimens were immersed in seawater (SW) at 40 °C. The weight change was periodically monitored using a precision balance (Five replicate specimens were used per measurement). The moisture content, M, (in percent) is calculated using,

$$M\% = \frac{W_t - W_o}{W_o} \times 100 \qquad (1)$$

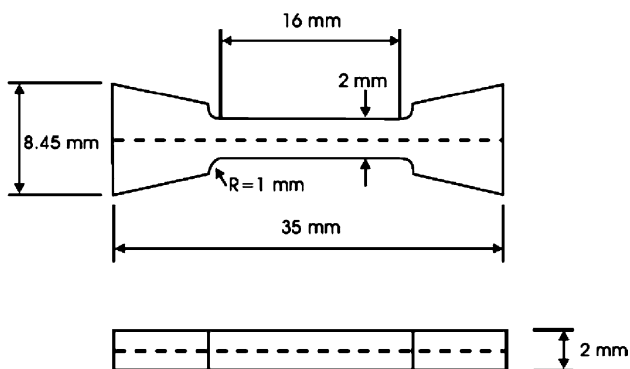where W_t is the measured weight of the specimen at time t and W_o is the specimen initial dry weight.

Table 1 Mechanical properties of E-glass fiber and vinylester matrix [7, 17, 18]

Fiber	
Axial modulus, E_{1f} (GPa)	73
Transverse modulus, E_{2f} (GPa)	73
Axial Poisson's ratio, v_{1f}	0.2
Fiber fracture toughness, Γ_f (J/m^2)	10
Diameter, d_f (μm)	14
Matrix	
Young's modulus, E_m (GPa)	2.7
Poisson's ratio, v_m	0.34
Strain to failure, ε (%)	8–10

Single fiber fragmentation test: modified procedure

The SFFT was conducted on dry and moisture saturated specimens. The SFFT specimen, Fig. 1, was loaded in tension using a small tensile stage (from Ernest F. Fullam, Inc.) equipped with a 1 kN capacity load cell. The tensile stage was placed under an optical transmission microscope (Olympus BX41 with a QICAM-FAST 1394 camera) and the specimen was examined using cross polarized light. The vinylester matrix resin is transparent which allows the use of photoelasticity to in situ analyze the distribution of stresses around a fiber break. When the loaded specimen is observed between crossed polarizers, the birefringence patterns, schematically illustrated in Fig. 2 [6], reveal that each fiber break is accompanied by a finite amount of F/M debonding (or instantaneous debonding). The intensity of the birefringence pattern over the debond zone near the fiber break is weak as a result of the low shear stress over the debonded region. The ends of the debonded region can be identified by the transition of the photoelastic pattern. The debond tip is located between the maximum width of the photoelastic pattern and the fiber break [19]. Birefringence patterns were therefore used to identify both the fiber break and the debond region around the fiber break.

We will first examine the energy release rate associated with the initial fracture event, viz., fiber fracture. The load required to achieve the first fiber break, P_f, was measured. The energy release rate, G_f, when the fiber breaks in the SFFT specimen is determined from the difference in

Fig. 1 Schematic representation of single fiber fragmentation test (SFFT) specimen [16]
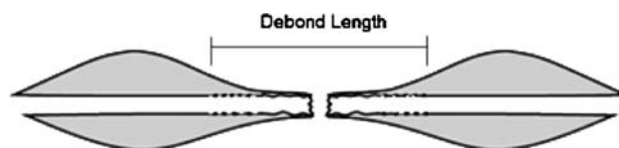

Fig. 2 Schematic representation of photoelastic patterns around a fiber break with F/M debonding

specimen compliance before and after the first fiber break occurs (derived in Ref. [15]),

$$G_f = \frac{4P_f^2 L_i}{\pi d_f^2} \left(\frac{1}{A_m E_m} - \frac{0.1478\pi A_1 d_f^2}{A_c A_m E_c E_m} - \frac{1}{A_c E_c} \right) \quad (2)$$

where A_m, A_c, E_m, and E_c are the cross-sectional areas and moduli of the matrix (m) and composite (c), respectively, d_f is the fiber diameter, L_i is the distance over which the fiber stress builds up after a fiber break to its far-field stress, and A_1 is a material parameter (see Appendix).

To determine just the debond fracture toughness, the attention is focused on an isolated debond propagation event. In order to circumvent analysis of the initial fiber fracture and debond propagation events and consider just debond propagation, the SFFT specimen was unloaded after the first break and instantaneous debonding occurred. The SFFT specimen was then loaded again until debond growth was observed, before any new fiber fracture occurred. The load, P_c, required to extend the existing debond was recorded and used to calculate the energy release rate associated with debond growth, G_{cd}, [15],

$$G_{cd} = \frac{P_c^2}{2\pi d_f} \left(\frac{1}{A_m E_m} - \frac{1}{A_c E_c} \right) \quad (3)$$

Notice, however, that there typically is a radial pressure, σ_R, acting on the F/M interface. This pressure arises from cure shrinkage of the resin and larger Poisson's contractions of the matrix than the fiber upon axial loading. Moisture induced swelling of the matrix will reduce the pressure. An expression for σ_R accounting for these factors, derived in Ref. [11], is provided in Appendix. As the debond grows, part of the fiber becomes unloaded, and the fiber and matrix will undergo sliding motions over the debonded region, and such motions are opposed by friction. The expression for the debond fracture toughness, $G_{cd}(\mu)$, taking into account friction is [15],

$$G_{cd}(\mu) = \frac{P_c^2}{2\pi d_f} \left(\frac{1}{A_m E_m} - \frac{1}{A_c E_c} \right) - \frac{\mu \sigma_R P_c L_{id}}{A_m E_m} \quad (4)$$

where μ is the coefficient of friction over the F/M interface debond zone. Notice that if friction is neglected ($\mu = 0$), the value of G_{cd} is an *apparent* fracture toughness value which neglects the energy dissipation due to friction between the fiber and matrix in the debonded region. G_{cd} ($\mu = 0$) will exceed the actual fracture toughness associated with debond propagation.

Results and discussion

Figure 3 illustrates a curve of weight change of E-glass/VE D8084 SFFT specimens immersed in seawater (SW) at
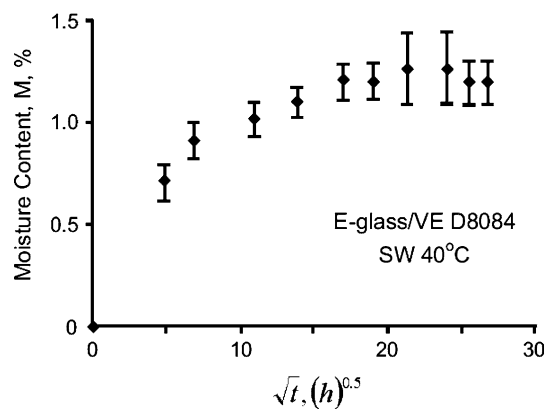

Fig. 3 Weight change for E-glass/vinylester SFFT specimens in seawater (SW) at 40 °C as function of square root of immersion time

40 °C versus square root of immersion time. The specimens reached moisture saturation ($M \approx 1.25\%$) after approximately 700 h of immersion.

Dry and moisture saturated (wet) SFFT specimens were loaded in tension until the first fiber break occurred. Figure 4 shows typical birefringence patterns observed after the first fiber break for dry and wet specimens. These birefringence patterns show that the fiber fracture is followed by an extremely large increment of debond growth in the water saturated specimens implying severe degradation of the F/M interface. The strain values in Fig. 4 were calculated from the load using; $\varepsilon = P/(A_c E_c)$.

The load required to break the fiber, P_f, and the instantaneous debond length, $2L_{id}$, obtained for dry and wet specimens are listed in Table 2. After immersion in water, the fiber breaks at a lower load since glass fibers degrade by exposure to water [7]. Results in Table 2 also show that the debond length is approximately 15 times larger after immersion in seawater as a result of severe F/M interface degradation. The scatter in debond length is substantial. After determining the fiber breaking load and the length of the instantaneous debond region, $2L_{id}$, the SFFT specimen was unloaded. Figure 5 illustrates photoelastic patterns in dry and wet specimens near the fiber break after the external load was removed. Even though the birefringence patterns partially disappeared after unloading the SFFT specimen, there are clear indications that the fiber/matrix interface was damaged by the energy released at the first fiber fracture.

The energy release rate, G_f, associated with fiber failure as calculated from Eq. 2 is listed for dry and wet SFFT specimens in Table 2. Nairn and Liu [10] reported that the corresponding energy release for T50 carbon fibers in an epoxy matrix at dry conditions is around 4.6 kJ/m² which is in reasonable proportion to the energy release rate determined for our lower strength glass fiber specimens

Fig. 4 Photoelastic pattern of the first fiber break in an E-glass/VE D8084 SFFT specimen; **a** dry and **b** wet
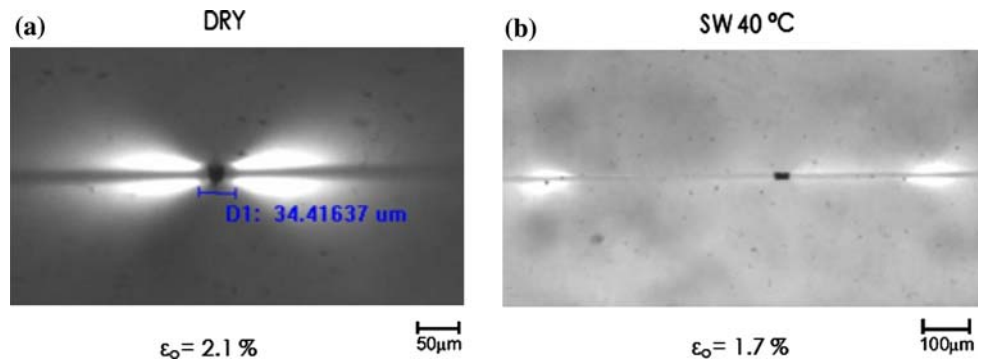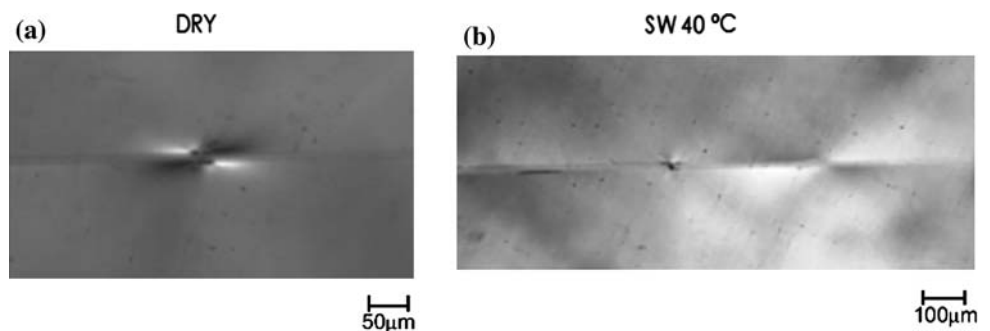

(a) DRY

D1: 34.41637 um

ε_o = 2.1 %

50μm

(b) SW 40 °C

ε_o = 1.7 %

100μm

Table 2 Energy release rate, G_f, associated with fiber failure at dry and wet conditions

	E-glass/VE D8084			
	A_c (mm^2)	P (N)	$2L_{id}$ (μm)	G_f (kJ/m^2)
DRY	4.0 ± 0.4	237 ± 9	48 ± 10	2.04 ± 0.44
SW 40 °C	3.9 ± 0.4	181 ± 6	618 ± 248	1.27 ± 0.07

(2.04 kJ/m^2). Nairn and Liu [10] argued that a minor fraction of this released energy is consumed by propagating a crack through the fiber, and attributed the additional energy released to initiation of fiber fracture, F/M debonding, and other dissipative processes.

After the first fiber fracture event, the SFFT specimen was unloaded and loaded again. As the load was increased, the F/M debond growth was monitored with the aid of photoelasticity. Figure 6 shows examples of photoelastic patterns near the fiber break at increasing levels of the externally applied strain (load) in dry (Fig. 6a) and wet (Fig. 6b) specimens. As indicated by the photoelastic patterns, the F/M interface is severely degraded after exposure to water, and the existing debond starts to propagate at a lower strain (load) than for the dry specimens. Representative curves depicting total debond length (both sides of fiber break) versus applied strain for the previously unloaded SFFT specimens are shown in Fig. 7. For the dry specimens, Fig. 7a shows that the existing debond starts to propagate at a strain very close to the strain at the first fiber break (i.e., $P_c \approx P_f$). For the specimens that were

immersed in seawater at 40 °C, the results in Fig. 7b show that the debond starts to propagate at a strain below that required to obtain the first fiber break (i.e., $P_c < P_f$). Table 3 lists the critical debond propagation loads (notice that $P_c = P_f$ was used for specimens at dry conditions). The *apparent* fracture toughness values, obtained by neglecting friction ($\mu = 0$), determined by substitution of the critical debond load, P_c, into Eq. 3 are listed in Table 3. Table 3 also includes previously reported [7] *apparent* F/M interface shear strengths for E-glass/VE D8084 at dry and wet conditions. The *apparent* debond fracture toughness ($\mu = 0$) was reduced by approximately 60% after exposure to seawater at 40 °C, which is similar to the reduction of the F/M interface shear strength (70%).

In order to quantify the influence of friction on the fracture toughness, it is necessary to determine the radial pressure at the F/M interface caused by residual stress introduced during cure shrinkage of the resin, σ_{RS}, moisture induced swelling of the matrix, σ_{RSW}, and differential Poisson's contractions of the fiber and matrix upon axial loading, σ_{RP}. The cure shrinkage strain was determined in a previous study [15]. Furthermore, the matrix swelling in sweater at 40 °C is $\varepsilon_{SW} = 0.22\%$. [20]. The Poisson contraction strain induced by differential Poisson ratios for the isotropic glass fiber and matrix was calculated as a function of applied load based on $v_{1f} = v_{2f} = 0.2$ and $v_m = 0.34$ obtained from Ref. [17].

The radial pressure components ($\sigma_{R,P}$, $\sigma_{R,S}$, and σ_{RSW}) at the F/M interface are calculated at the critical load for debond propagation as described in the Appendix. Table 4

Fig. 5 Photoelastic pattern near fiber break point after unloading; **a** dry and **b** wet E-glass/VE D8084 SFFT specimens

(a) DRY

50μm

(b) SW 40 °C

100μm

Fig. 6 Photoelastic patterns near a fiber break at increasing levels of applied strain; **a** dry and **b** wet E-glass/VE D8084 SFFT specimens
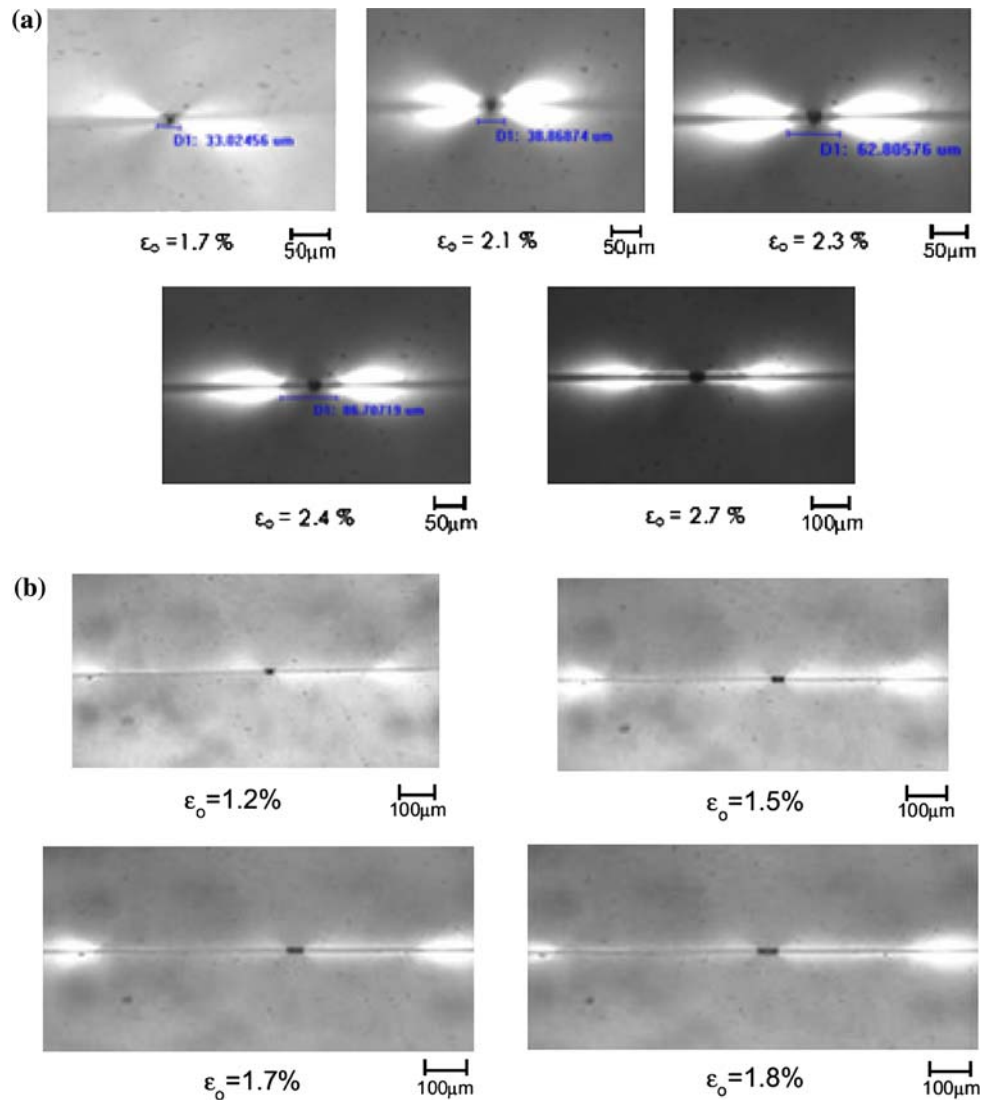
presents the results of the radial pressure components and the magnitude of total radial pressure at the interface obtained from Eqs. 12–15. The results in Table 4 show that residual stress introduced by the cure shrinkage of the vinylester resin is the dominating factor for the radial pressure.

Fracture toughness values, calculated from Eq. 4, for a range of coefficients of friction ($\mu = 0$–1) are summarized in Table 5. When friction is considered, the fiber/matrix interface fracture toughness is reduced since the *apparent* fracture toughness includes the frictional work. Notice that friction has a very large effect on the interface fracture toughness of the specimens immersed in seawater since the debond lengths are extremely large (approximately 15 times larger than for the dry specimens, Table 2 and Fig. 6). Therefore, large values for the coefficient of friction will imply that a large amount of energy is consumed in frictional work and thus it will significantly decrease the values of the actual interface fracture toughness.

Without a known value of the coefficient of friction over the debonded region of the fiber/matrix interface, it is not possible to appropriately determine the interface toughness. Several researchers [21, 22], however, have estimated values for the coefficient of friction at the interface at dry conditions. Chua and Piggott [21] report coefficient of friction for dry glass/epoxy between 0.5 and 0.8. A coefficient of friction of 0.8 in Eq. 4 gives an interface fracture toughness $G_{cd} = 47.9 \pm 20$ J/m^2 for the E-glass/VE D8084 specimens at dry conditions. Chua and Piggott report a fracture toughness, G_{cd}, of 50 J/m^2 (dry conditions) for glass/epoxy (based on pull-out testing) which is close to the fracture toughness of glass/vinylester found in this study.

To the author's knowledge, information regarding values for the coefficient of friction at the interface of specimens subjected to water has not been published. The coefficient of friction, however, must be less than 0.3. Otherwise, according to this analysis, it would not be
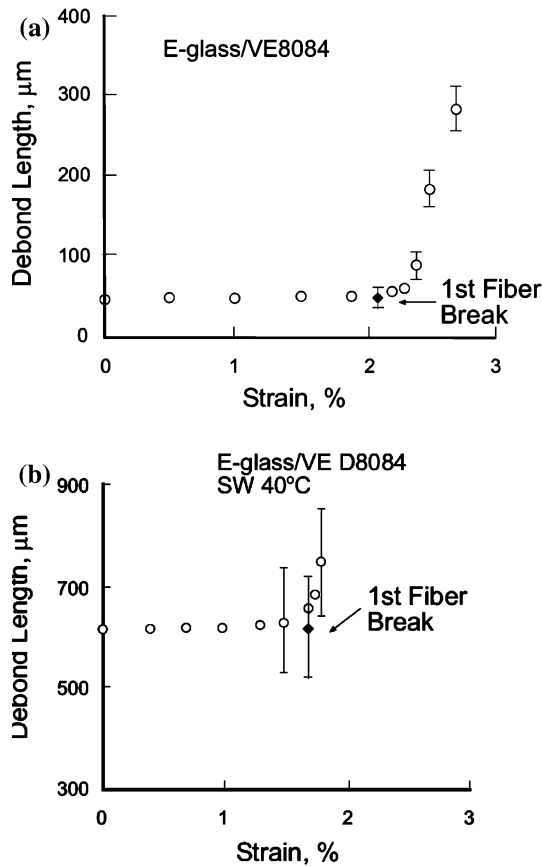
(a) E-glass/VE8084

(b) E-glass/VE D8084 SW 40°C

Fig. 7 Total debond length as a function of applied strain; **a** dry and **b** wet E-glass/VE D8084 SFFT specimens. The filled diamond-shaped symbol represents the instantaneous debond length (1st loading), and the open circles represent debond length measured during the 2nd loading

Table 3 SFFT results: apparent debond fracture toughness and F/M interface shear strength

	E-glass/VE D8084		
	P (N)	G_{cd} (J/m^2)	τ (MPa) [7]
DRY	237 ± 9	62 ± 13	63.0 ± 25.1
SW 40 °C	153 ± 16	27 ± 7	19.5 ± 13.9

Table 5 Effect of friction on the interface fracture toughness: dry conditions: $P_c = 237$ N, $2L_{id} = 48$ μm, $\sigma_R = 32$ MPa, and $A_c = 4$ mm^2; wet conditions: $P_c = 153$ N, $2L_{id} = 618$ μm, $\sigma_R = 25$ MPa, and $A = 3.9$ mm^2 (averages)

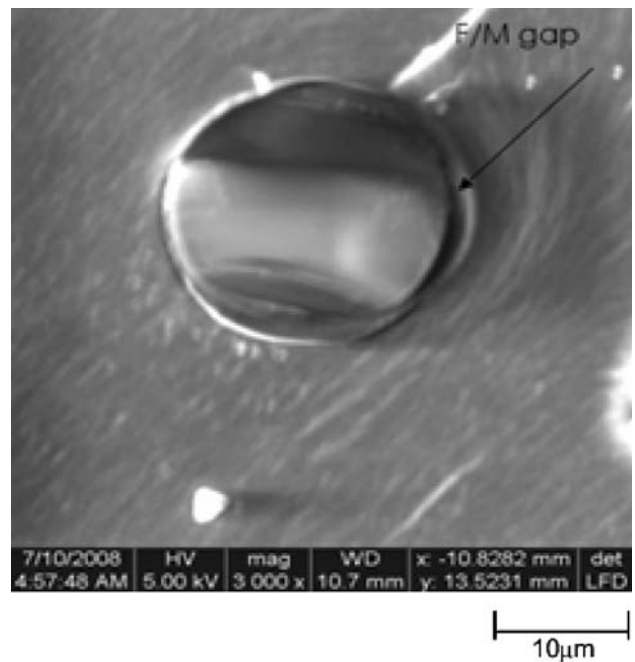| μ	G_{cd} (J/m^2)	
	Dry	SW 40 °C
0	61.5	26.9
0.1	59.7	15.8
0.2	58.1	4.6
0.3	56.4	–
0.5	53	–
0.8	47.9	–
1.0	44.5	–

Fig. 8 ESEM micrograph of a cross section of a wet E-glass/VE D8084 SFFT specimen

possible to propagate the debond (Table 5). Moreover, it might be possible that the F/M interface is so degraded by water that the specimen has a relative open interface

(frictionless). To examine this hypothesis, cross-sections of wet SFFT specimens were inspected in an environmental scanning electron microscope (ESEM). Figure 8 shows an example of an ESEM micrograph of a cross section of a

Table 4 Total radial pressure at the F/M interface ($|\sigma_R|$) caused by the differential Poisson's contractions of the fiber and matrix upon axial loading (σ_{RP}), residual stress introduced during cure shrinkage of the resin (σ_{RS}), and moisture induced swelling of the matrix (σ_{RSW})

	E-glass/VE D8084			
	σ_{RP}, MPa (ε_o, %)	σ_{RS}, MPa (ε^*, %)	σ_{RSW}, MPa (ε_{SW}, %)	$|\sigma_R|$ (MPa)
DRY	−6 (2.2)	−26 (1.1)	0 (0)	32
SW 40 °C	−4 (1.5)	−26 (1.1)	5 (0.22)	25

The quantity in parenthesis is the associated linear strain

wet E-glass/VE D8084 SFFT specimen. The microphotograph shows the presence of a relative large gap between the fiber and the matrix indicating a severely degraded interface, lack of contact and hence a frictionless interface. This hypothesis is also supported by water absorption data for vinylester matrix composites where the F/M interface was found to dominate the water uptake (wicking) [7].

Conclusions

The main objective of this work was to utilize a revised single fiber fragmentation test to characterize the influence of water absorption on the F/M interface fracture toughness of E-glass/VE D8084. Experiments were performed on dry and wet SFFT specimens. The fracture toughness values obtained for dry SFFT specimens, $G_{cd} = 62$ J/m^2 (apparent-frictionless) and 48 J/m^2 (friction), are in good agreement with toughness data determined for glass/epoxy by other investigators and test methods. After immersion in seawater, large extents of F/M debonding observed in the SFFT specimens indicate that the interface was severely degraded. Moreover, ESEM microphotographs taken of cross sections of the SFFT specimens confirm that interface degradation leads to relative large gaps between the fiber and the matrix. The fracture toughness value obtained for the SFFT specimen after immersion in seawater, $G_{cd} = 27$ J/m^2 (frictionless), represents a substantial reduction in interface fracture toughness from the dry state. The fracture toughness was reduced to a similar extent as the interface shear strength by exposure to seawater.

Appendix

Ineffective length, L_i, material and specimen properties

The zone over which the fiber stress builds up to its far-field value has been termed the *ineffective zone*. The length of this zone, L_i, is defined as the distance required to recover the stress in the fiber to 95% of the far-field stress [23] (the total ineffective length is $2L_i$). The ineffective length, L_i, is provided by an axisymmetric model of the SFFT developed by Whitney and Drzal [23]:

$$L_i = 2.375 \frac{d_f}{2} \sqrt{\frac{E_{1f}}{G_m} - 4v_{1f}} \tag{5}$$

A_1 is a material property constant for the combination of fiber and matrix given by,

$$A_1 = E_{1f} + \frac{4K_f G_m v_{1f}}{(K_f + G_m)}(v_{1f} - v_m) \tag{6}$$

where K_f is the plane strain bulk modulus of the fiber,

$$K_f = \frac{E_{2f}}{2(2 - E_{2f}/2G_{2f} - 2v_{2f}E_{2f}/E_{1f})} \tag{7}$$

where E_{1f}, E_{2f}, v_{1f}, and v_{2f} are the axial and transverse moduli and Poisson's ratios of the cylindrically orthotropic fiber (glass fibers are isotropic), G_{2f} is the transverse shear modulus of the fiber, and G_m is the shear modulus of the matrix.

The cross sectional area, A_c, and effective Young's modulus, E_c, of the SFFT specimen are:

$$A_c = d^2 \tag{8}$$

$$E_c = V_f E_{1f} + V_m E_m \tag{9}$$

where d is the side length of the square cross section of the SFFT specimen, E_m is the Young's modulus of the matrix, and V_f and V_m are the volume fraction of the fiber and matrix calculated as:

$$V_f = \frac{A_f}{A_c} \text{ and } V_m = \frac{A_m}{A_c} \tag{10a, b}$$

where A_f and A_m are the cross section areas of fiber and matrix in the SFFT specimen,

$$A_f = \frac{\pi}{4} d_f^2 \text{ and } A_m = A_c - A_f \tag{11a, b}$$

Radial pressure, σ_R, at the fiber/matrix interface

The radial pressure, σ_R, at the F/M interface is caused by cure shrinkage introduced during cure of the resin, differential Poisson's contractions of the fiber and matrix upon axial loading, and moisture induced swelling of the matrix. Assuming that the fiber is embedded in an infinite matrix, the radial pressure due to Poisson contraction of fiber and matrix, $\sigma_{R,P}$ is given by [11]:

$$\sigma_{R,P} = -\frac{\varepsilon_o(v_m - v_{1f})}{\frac{(1-v_{2f})}{E_{2f}} + \frac{(1+v_m)}{E_m} - \frac{2v_{1f}^2}{E_{1f}}} \tag{12}$$

where the far field strain applied to the SFFT specimen is given by $\varepsilon_o = P/(A_c E_c)$ and v_m is the Poisson ratio of the matrix.

The radial pressure, $\sigma_{R,S}$, caused by matrix cure shrinkage is [11]:

$$\sigma_{R,S} = -\frac{\varepsilon^*(1 + v_{1f})}{\frac{(1-v_{2f})}{E_{2f}} + \frac{(1+v_m)}{E_m} - \frac{2v_{1f}^2}{E_{1f}}} \tag{13}$$

where ε^* is the magnitude of the matrix cure shrinkage after the gel point of the resin expressed as a linear strain.

The radial pressure, $\sigma_{R,SW}$, caused by moisture-induced swelling of the matrix is [11]:

$$\sigma_{R,SW} = \frac{\varepsilon_{SW}(1 + v_{1f})}{\frac{(1 - v_{2f})}{E_{2f}} + \frac{(1 + v_m)}{E_m} - \frac{2v_{1f}^2}{E_{1f}}} \tag{14}$$

where ε_{SW} is the moisture-induced swelling of the matrix expressed as a linear strain.

The magnitude of the total compressive radial pressure, $\left|\sigma_{R,P} + \sigma_{R,S} + \sigma_{R,SW}\right|$, at the interface is then,

$$\sigma_R = \left| \frac{\varepsilon_{SW}(1 + v_{1f}) - \varepsilon_o(v_m - v_{1f}) - \varepsilon^*(1 + v_{1f})}{\frac{(1 - v_{2f})}{E_{2f}} + \frac{(1 + v_m)}{E_m} - \frac{2v_{1f}^2}{E_{1f}}} \right| \tag{15}$$

References

1. Ray BC (2006) J Colloid Interface Sci 298:111
2. Rao V, Herrera-Franco PJ, Ozzelo AD, Drzal LT (1991) J Adhesion 34:65
3. Cox HL (1952) Br J Appl Phys 3:72
4. Kelly A, Tyson WR (1965) J Mech Phys Solids 13:329
5. Drzal LT, Rich MJ, Camping JD, Park WJ (1980) Proceedings of 35th annual technical conference reinforced plastics/composites institute, Paper 20-C:1. SPI, New Orleans
6. Kim BW, Nairn JA (2002) J Compos Mater 36:1825
7. Ramirez FA, Carlsson LA, Acha BA (2008) J Mater Sci 43:5230. doi:10.1007/s10853-008-2766-z
8. Cervenka AJ, Young RJ, Kueseng K (2005) Compos Part A 36:1020
9. Kobiki A, Kawada H (2005) JSME Int J Series A: Solid Mech Mater Eng 48:183
10. Nairn JA, Liu YC (1996) Compos Interfaces 4:241
11. Nairn JA, Liu YC (1997) Int J Solids Struct 34:1255
12. Nairn JA (2000) Int J Fract 105:243
13. Liu HY, Mai YW, Ye L, Zhou LM (1997) J Mater Sci 32:633. doi:10.1023/A:1018527516621
14. Wagner HD, Nairn JA, Detassis M (1995) Appl Compos Mater 2:107
15. Ramirez FA, Carlsson LA, Acha BA (2008) Compos Part A (in press)
16. Feih S, Wonsyld K, Minzari D, Westmann P, Liholt H (2004) Testing procedure for the single fiber fragmentation test. Riso National Laboratory, Riso-R-1483(EN), Roskilde, Denmark
17. Daniel IM, Ishai O (2006) Engineering mechanics of composite materials. Oxford University Press, New York
18. Harris B, Morley J, Phillips DC (1975) J Mater Sci 10:2050. doi:10.1007/BF00557483
19. Kim BW, Nairn JA (2002) J Mater Sci 37:3965. doi:10.1023/A:1019684312272
20. Ramirez FA (2008) Master's Thesis. Department of Mechanical Engineering Florida Atlantic University, Florida
21. Chua PS, Piggott MR (1985) Compos Sci Technol 22:185
22. Baillie C (1991) PhD Thesis. Department of Materials Science and Engineering University of Surrey, Surrey
23. Whitney JM, Drzal LT (1987) Toughened Compos ASTM STP 937:179